Research Journal of Applied Sciences 13 (10): 616-625, 2018
ISSN: 1815-932X

Synthesis, Crystal Structure, Optical Properties and the Theoretical Study of a Photo-Switchable 8-(*p*-tolyl)-8*H*-Acenaphtho [1, 2-*d*] Imidazolyl Dimer

[1]Al-Anood M. Al-Dies, [1,2]Abdullah M. Asiri, [1]Osman I. Osman and [1]Salman A. Khan
[1]Department of Chemistry,
[2]Center of Excellence for Adavanced Materials Research (CEAMR), Faculty of Science,
King Abdulaziz University, 21589 Jeddah, Saudi Arabia

Abstract: The X-ray structure analysis show that the radical dimerization of 8-(*p*-tolyl)-8*H*-acenaphtho [1, 2-*d*] imidazole leads to 1, 2'-isomer structure. The estimated geometrical parameters are in excellent agreement with the experimental crystal structural peers. 8-(*p*-tolyl)-8*H*-acenaphtho [1, 2-*d*] imidazolyl dimer (TAID) exhibited excellent photochromism. The colored species of TAID are stable in solutions with good fatigue resistance. Its kinetic studies show that the photocoloration obey first order kinetics and the thermal bleaching processes obey second order. The photochromic dye shows decrease of fluorescence intensity with the photochromic reaction, due to the formation of nonemissive photoproduct and with the thermal recombination reaction in the dark the fluorescence intensity recovers.

Key words: Photodissociation, thermal recombination, kinetics, fluorescence switching, X-ray, DFT

INTRODUCTION

Organic photochromic dyes with interest properties are industrially important, the largest current application of photochromic dyes is ophthalmic lens (Dessauer, 2006). Photochromism was first recognized by Markwald in 1899. Photochromic molecules have the ability to change color upon UV light irradiation. There are many classes of organic photochromic molecules for example, spiropyrans (Bulanov *et al*., 2003) benzopyrans (Coelho *et al*., 2005) diarylethenses (Shirinian *et al*., 2014; Ohshima *et al*., 2015) fulgides (Bahajaj and Asiri, 2007; Islamova *et al*., 2008; Slavov *et al*., 2015) fulgimide (Nithyanandan and Kannan, 2013) salicylideneaniline (anils) (Robert *et al*., 2010; Koshima *et al*., 2011) azobenzene, stilbenes (Bandara and Burdette, 2012) and Hexaarylbiimidazole (HABI) (Mutoh *et al*., 2012; Edkins *et al*., 2014; Iwasaki *et al*., 2014; Yamaguchi *et al*., 2015). The photochromism of these photochromic molecules has been employed commercially and it one of the most industrially funded research area (Corns *et al*., 2009). HABI was discovered in the 1960s by Hayashi and Maeda through the oxidation of 2, 4, 5-triphenylimidazole (TPI) (Nakamura and Irie, 1988). TPI is the first chemiluminescent molecule that was discovered by Radziszewski (1877). Under UV light, HABI forms a pair of colored TPI radicals due to cleavage of the C-N bond. Additionally, TPI radicals can be formed under high pressure and temperature, under these conditions this organic photochromic molecule becomes different from other photochromic materials (Koko and Taro, 1970; Cohen, 1971; Coraor *et al*., 1971; Kikuchi *et al*., 2002). The fluorescence technique has many range of applications in numerous fields, photo-switchable molecules have been wide applications in optical memory and bio-imaging (Zhu *et al*., 2010, 2011). Their application in super-resolution imaging in particular, relies on the reversible transformation between the fluorescent "ON" and "OFF" states after photo-excitation of the photo-switchable molecule. Apart from color change associated with the photoinduced transformation of photochromic compound, structural changes during photochromic reaction can also, change the molecule emission (Irie, 2000). In most instances, only one form of the interconverting states has high fluorescence quantum yield. The emission intensity of a photochromic compound can be modulated. A multifunctional HABI switches derived from 9-ethyl-9*H*-carbazole, chloro-substituted phenyl and piperonal were previously reported by our group (Asiri *et al*., 2005, 2009; Asiri and Badahdah, 2006) and found to have piezochromism, thermochromism and photochromism properties in different solvents. In this study, we report the synthesis of a novel photochromic *p*-tolyl-acenaphthoimidazole dimer (TAID) together with the experimental and theoretical study.

Corresponding Author: Al-Anood M. Al-Dies, Department of Chemistry, Faculty of Science, King Abdulaziz University, 21589 Jeddah, Saudi Arabia

MATERIALS AND METHODS

^{1}H and ^{13}C NMR spectra were recorded at 850 MHZ on a Bruker AVANCE ™ III HD, $CDCl_3$ was used as deuterated solvent. Mass spectra (DART-ToFMS) were measured by using a AccuToF LC-plus JMS-T100LP (Joel). IR spectra were measured on a Perkin Elmer FT-IR spectrometer. UV-Visible spectra were recorded on evolution 300 spectrometer. Fluorescent spectra were recorded on HITACHI f-7000 Fluorescence spectrophotometer. Melting point were determined with a Stuart Scientific Co. Ltd., Apparatus. The molecular structure identified with ^{1}H and ^{13}C NMR, MS, IR and X-ray are provided in electronic supplementary material.

Computational analysis: The Density Functional Theory (DFT) calculations were done applying the Gaussian 09 Suites of programs (Frisch *et al*., 2009) together with the GaussView (Milliam *et al*., 2007) for investigating the geometry of TAID. Version 3.1 of Natural Bond Orbital (NBO) program (Reed *et al*., 1988) was used to study the electric charges and the delocalization interactions of TAID. The molecular structure of TAID was optimized applying the hybrid Becke's 3 parameter Lee-Young-Parr correlation functional (CAM-B3LYP) (Yanai *et al*., 2004) of DFT with double-zeta and polarization functions on heavy atoms basis set [6-31+G*]. A global minimum on the potential energy surface of TAID was located and confirmed by the absence of any imaginary vibrational wavenumber. The ultra-violet spectra of TAID in chloroform ($CHCl_3$) and benzene (C_6H_6) were simulated using Time-Dependent Density Functional Theory (TD-DTF) (Gross and Kohn, 1990) and the Polarizable Continuum Model (PCM) method (Cances *et al*., 1997) with the 6-31+G* basis set.

Experimental section

Synthesis of 8-(*p*-tolyl)-8*H*-acenaphtho [1, 2-*d*] imidazole (TAI): p-tolualdehyde (3 g, 25 mmol), acenaphthylene-1, 2-dione (4.55 g, 25 mmol) and ammonium acetate (13.47 g, 174.78 mmol) were stirred in acetic acid (50 mL) under reflux for 6 h in an oil bath (TLC) monitoring. Then the reaction mixture was cooled to room temperature and poured into an ice-cooled water and neutralized with sodium bicarbonate to result in formation of an orange precipitate. Recrystallization of the orange product from benzene/ethanol gave TAI as an orange powder (Fig. 1). Yield: 56%; m.p.: 133-134°C; IR ν_{max}/cm^{-1} : 3435 ($NH_{stretch}$), 1515 (NH_{bend}), 3112, 3086, 3041 ($CH_{aromatic\ stretch}$), 1683 (C = N), 1609, 1476 (C = C), 1348 (C-N), 2914 ($CH3_{stretch}$), 1445, 1375 ($CH_{3\ bend}$); ^{1}HNMR (850 MHz, $CDCl_3$-d, δ_{ppm}): 9.890 (s, 1H, NH), 8.683 (t, J = 7.9 Hz, 1H), 8.526 (d, J = 7.1 Hz, 1H), 8.184 (d, J = 7.9 Hz, 1H), 7.803-7.735 (m, 1H), 7.727-7.692 (m, 1H), 7.604 (d, J = 8.2 Hz, 2H), 7.305 (t, J = 6.1 Hz, 1H), 7.262 (d, J = 7.9 Hz, 2H), 2.367 (s, 3H, CH_3); ^{13}C NMR (213 MHz, $CDCl_3$-d, δ_{ppm}): 140.02, 134.70, 131.56, 131.11, 129.88, 129.73, 129.70, 129.38, 128.95, 128.20, 127.89, 127.45, 126.97, 125.08, 123.93, 122.53, 122.10, 121.40, 120.15, 30.96; MS (DART-ToFMS) m/z: calculated 282.35, found 282.30 g/mole with a base peak at 282.11.

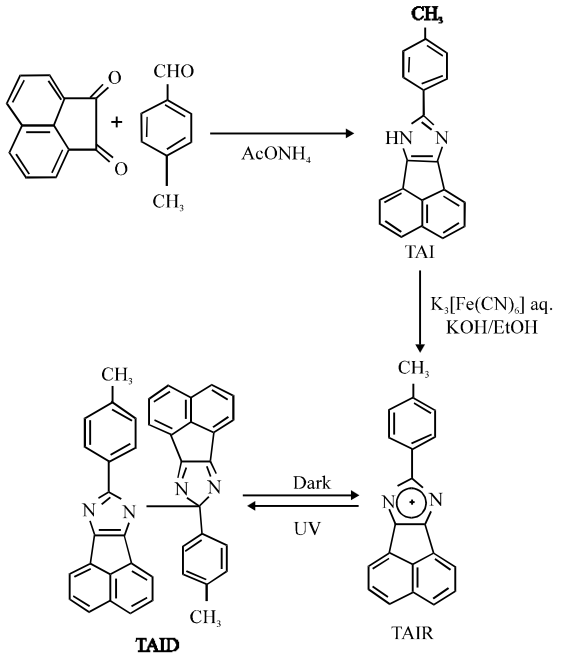

Scheme 1: Synthesis route to TAID

Synthesis of 8, 8'-di-*p*-tolyl-8'*H*-7, 8'-bi aenaphtho [1, 2-*d*] imidazole (TAID): The synthetic method for preparing TAID was reported in the literature (White and Sonnenberg, 1966) (Fig. 1). A solution of TAI (1 g, 3.54 mmol) was added to 2N ethanolic potassium hydroxide (100 mL) and placed in an ice bath. With exclusion of light, a freshly prepared 2% aqueous solution of potassium ferricyanide (500 mL) was gradually added during a period of 1.5 h with stirring. The reaction mixture was stirred overnight at room temperature. The precipitate was filtered, washed with water repeatedly and then dried in a vacuum. Yield: 67%; m.p.: 246-248°C; IR ν_{max}/cm^{-1} : 3023, 2969, 2917 ($CH_{aromatic\ stretch}$), 2860($CH_{3\ stretch}$) 1429, 1369 ($CH_{3\ bend}$), 1638 (C = N), 1608, 1484 (C = C) and 1281 (C-N); ^{1}HNMR (850 MHz, $CDCl_3$-d, δppm): 8.107 (dd, J = 6.3 and 9.4 Hz, 2H), 7.851 (d, J = 7.3 Hz, 2H), 7.783 (t, J = 7.3 Hz, 2H), 7.654 (dd, J = 8.4 Hz, 2H), 7.487 (t, J = 6.3 Hz, 2H), 7.458 (d, J = 7.9 Hz, 2H), 7.381-7.348 (m, 2H), 7.287 (d, J = 7.9 Hz, 2H), 7.072 (d, J = 7.9 Hz, 2H), 6.902 (d, J = 7.9 Hz, 2H), 2.305 (s, CH_3);13 C NMR (213 MHz, $CDCl_3$-d, δ_{ppm}):

171.50, 153.05, 149.56, 147.53, 139.60, 138.07, 137.03, 134.04, 131.55, 131.31, 130.51, 130.39, 129.23, 128.62, 127.80, 127.24, 127.06, 125.36, 123.90, 21.30; MS (DART-ToFMS) m/z: calculated 562.66, found 563.62 g/mole with a base peak at 283.12.

RESULTS AND DISCUSSION

X-ray crystallographic analysis: A single crystal of TAID, suitable for X-ray crystallographic analysis was obtained by recrystallization from benzene/ethanol. The CIF of TAID has been submitted to Cambridge Crystallographic Data Center (CCDC) with the CCDC number 1846947. The X-ray analysis shows that TAID has 1, 2'-isomer structure in which a C-N bond joins the 1- and 2'-positions of the 2 imidazole rings (Fig. 2). The C-N bond of 1.468 (2) Å as a most remarkable structural feature of TAID has a length quite consistent with that connecting the 2 imidazole rings of HABI derivatives (Edkins *et al*., 2014; Hatano *et al*., 2010; Masaki *et al*., 2000).

Geometrical parameters: Figure 3 depicts the optimized geometry and atom numbering of TAID using CAM-B3LYP/6-31+G* level of theory. Table 1 shows some bond lengths and angles of the optimized structure of gas-phase TAID dye. It is of interest to extract some structural remarks from Table 1 and Fig. 3: TAID dye is composed of 2 imidazolyl moieties, Im1 and Im2. The former is semi-planar with a dihedral angle of 131.6° between the benzene and the acenaphthalo-imidazolyl rings while the later has an sp^3 carbon atom that completely distorts planarity between the benzene and acenaphthalo-imidazolyl rings, the estimated geometrical parameters are in excellent agreement with the experimental crystal structural peers, the maximum errors encountered in bond lengths and angles do not exceed 0.99 and 2.46%, respectively, the computed C-N bond that characterizes the connection 3 between the 2 imidazolyl rings agrees nicely with the crystal structure value of 1.478 Å, the relatively high discrepancies encountered in the dihedral angles could be due to phase difference i.e., the computed geometrical parameters are of gas-phase origin while the experimental ones are solid state values, the computed and measured bond angles of 107-128° indicate clearly the C = C and C = N sp^2 hybridization scheme over most parts of the TAID dye.

Photochromic properties: The colorless TAID in chloroform solution, shows 2 absorptions with maxima at 296 and at 378 nm (Fig. 4). After UV irradiation, the absorbance at 378 nm increase in addition to a new absorption band in the visible region (λ_{max} = 556 nm) and the solution turned light red. These new bands can be ascribed to the 8-(*p*-tolyl)-8*H*-acenaphtho [1, 2-*d*] imidazolyl radical (TAIR) (Fig. 4). This photochromic behavior is attributed to the photoinduced homolytic cleavage of the C-N bond between the imidazole rings. The color of TAIR in chloroform gradually reverted to the original color on standing in the dark at room temperature

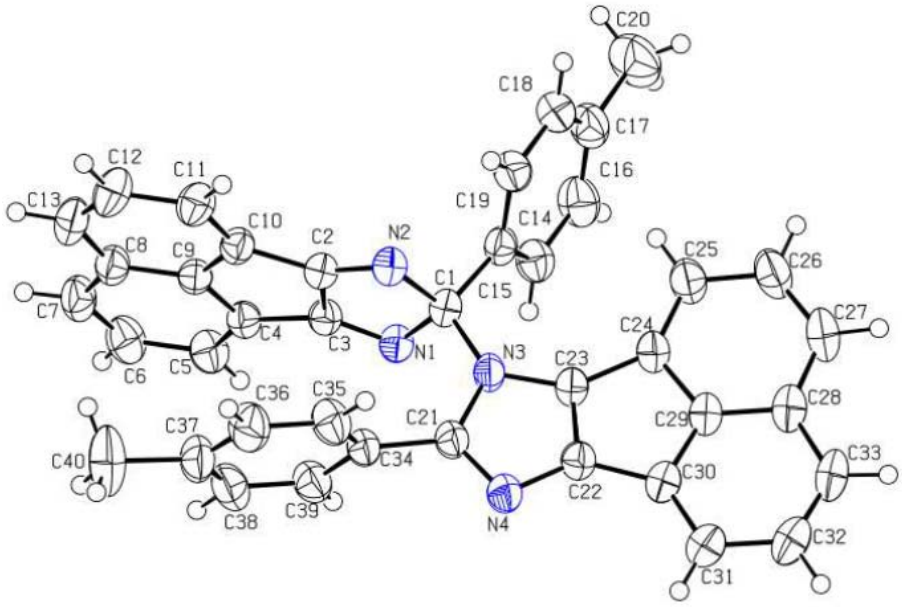

Fig. 2: ORTEP diagram of TAID, thermal ellipsoids were drawn at 50% probability level

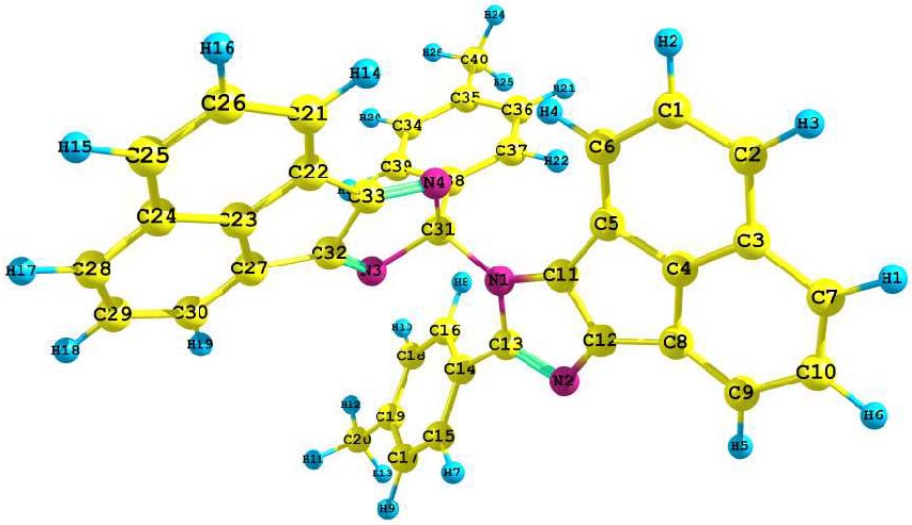

Fig. 3: The atom number of the optimized structure of TAID using CAM-B3LYP/631+G* level of theory

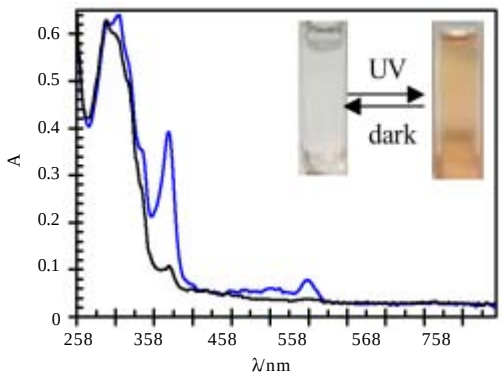

Fig. 4: Absorption spectrum and color changes of TAID in $CHCl_3$ ($c = 10^{-4}$ M) before UV irradiation (black line) and after 365 nm UV irradiation (blue line)

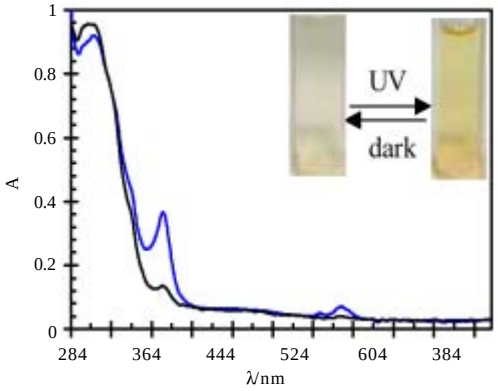

Fig. 5: Absorption spectrum and color changes of TAID in C_6H_6 ($c = 10^{-4}$ M) before UV irradiation (black line) and after 365 nm UV irradiation (blue line)

Table 1: The bound lenghts (Å) and angles (degrees) for TAID estimated by using CAM-B3LYP/631+G* level of theroy compared with their structures counterparts

Parameters	Crystal	B3LYP/631+G*	Error (%)
r_{C31-N1}	1.468	1.478	0.68
r_{C31-N3}	1.510	1.503	0.46
r_{C31-N4}	1.492	1.489	0.20
$r_{C31-C38}$	1.518	1.533	0.99
r_{N1-C11}	1.389	1.391	0.14
$r_{N1-C131}$	1.397	1.410	0.93
$r_{C31-C14}$	1.467	1.477	0.68
r_{C32-N3}	1.278	1.281	0.23
r_{C33-N4}	1.278	1.280	0.16
$<_{N1-C31-N4}$	109.8	107.1	2.46
$<_{N1-C31-N3}$	109.4	108.6	0.73
$<_{N4-C31-N3}$	109.0	108.7	0.27
$<_{N1-C13-N2}$	112.4	111.6	0.71
$<_{N2-C13-C14}$	122.7	120.8	1.55
$<_{N1-C13-C14}$	124.7	127.6	2.33
$<_{N1-C31-C14-C16}$	131.6	180.0	26.90

and the absorption of the new bands disappear by radical recombination to result in the recovery of the parent dimer. A similar photochromic behavior was also observed in benzene solution before UV irradiation, absorption peaks in the UV-region at 300 and 375 nm were observed (Fig. 5). Under UV irradiation the solution turned light orange with increase in the absorption peak at 375 nm and new absorption peak appear at 552 nm (Fig. 5).

The photo-coloration and thermal bleaching processes were readily followed spectrally at measured time intervals and they were found to obey first and second-order rate equations, respectively. The integrated form of the first-order rate law for the photodissociation process is:

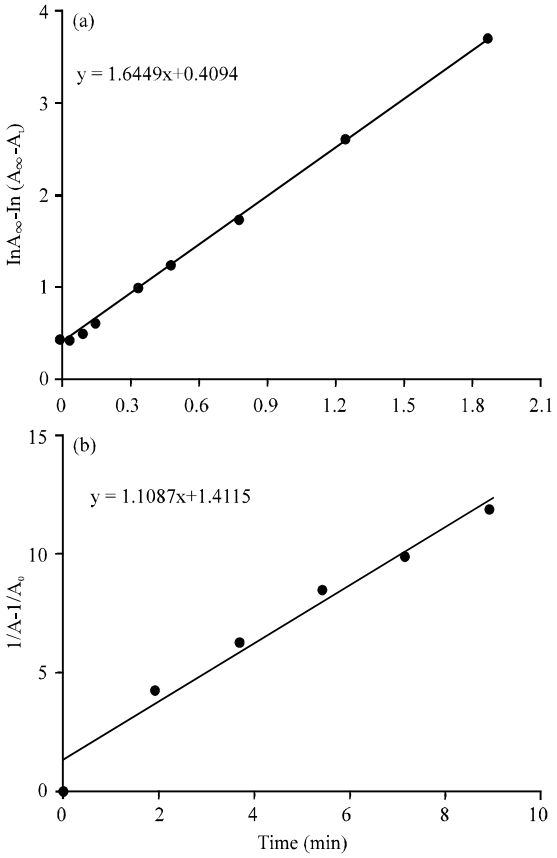

Fig. 6: a) First-order rate plot for the photo dissociation process of TAID and b) Second-order rate plot of thermal recombination process in C_6H_6 (c = 10^{-4} M)

$$\ln\frac{A_\infty}{A_\infty - A_t} = kt \quad (1)$$

Where:

k = The rate constant

A_∞ = The absorbance of the photoradicals at infinite time

A_t t = Its absorbance at time t

Plot of [ln (A_∞)-In (A_∞-A_t)] against time, gives a straight line with slope equals k. In the second-order rate equations, linear plots of (1/A-1/A_0)versus t were obtained until the absorbance A was about half of the absorbance of the radical species (A_o) when deviations from a second-order plot became apparent. In Fig. 6 the first-order rate plot for the photodissociation process and second-order rate plot of thermal recombination process in C_6H_6, the rate constants and half-lives are shown in Table 2. It is clear from Table 2 that the photodissociation yield is higher in chloroform, however, in chloroform the photodissociation was slow compare to that in benzene. Whilst the thermal recombination is almost identical in all solutions. The thermal recombination is much slower than photocoloration due to the stability of the radical species in solution.

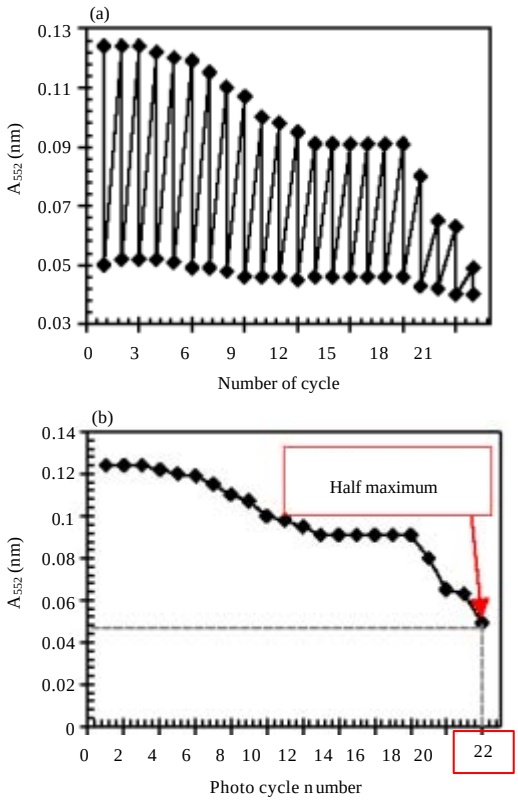

Fig. 7: a) Switching cycles for TAID monitored at 552 nm in C_6H_6 (c = 10^{-4} M) and b) The maximum cycle absorbance for many subsequent cycles with photodissociation process

Table 2: The rate constants, half-lives and photodissociation yield of TAID

Variables	k (min^{-1})	$t_{1/2}$(min)	Φ_{diss}
Photocoloration			
C_6H_6	164.49×10^{-2}	0.42	0.052
$CHCl_3$	43.12×10^{-2}	1.60	0.084
Thermal recombination			
C_6H_6	110.87×10^{-2}	7.39	
$CHCl_3$	169.52×10^{-2}	7.47	

Fatigue resistance: Fatigue resistance is an important property for photochromic materials to possess. The photochromic molecule to work as a switch should be able to undergo a large number of cycles. 39.5% non decomposed of TAID after 22 repetitive switching cycles (Fig. 7a) by irradiation of benzene containing TAID for 80 s and then the radicals kept in darkness for 10 min as one cycle. A typical sign of photo-degradation is the decreasing intensity of the radical species upon repetitive UV irradiation where the absorbance decreased to 50% after 22 cycles (Fig. 7b).

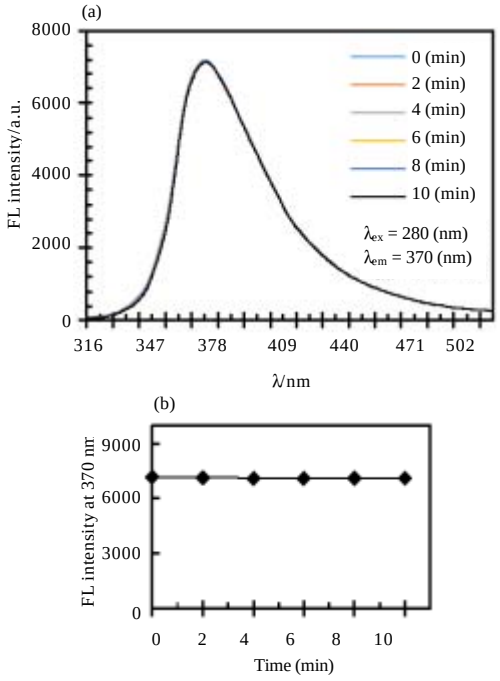

Fig. 8: a) FL spectra changes with scanning time and b) Changes of FL intensity with scanning time of TAID at 280 nm excitation in C_6H_6 (c = 5×10^{-5} M)

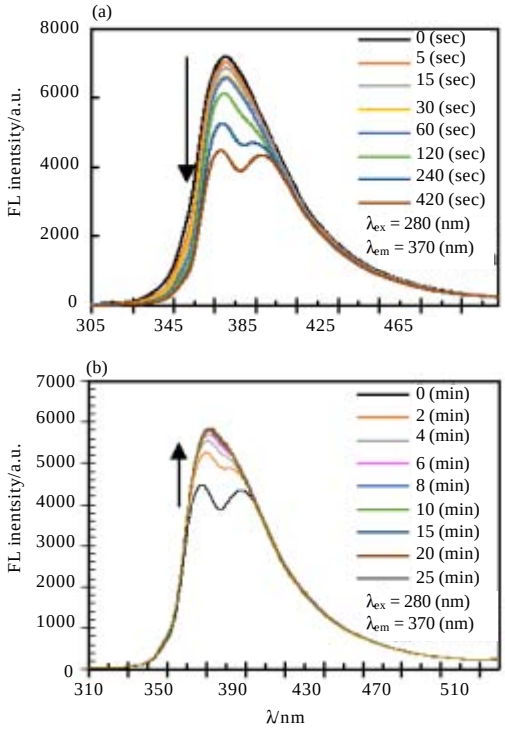

Fig. 9: a) FL spectra changes of TAID upon UV irradiation and b) FL spectra changes with fading time in darkness (λ_{irr} = 365 nm, λ_{ex} = 280 nm, c = 5×10^{-5} M in C_6H_6)

Fluorescence switching: Upon UV light excitation, TAID decomposes into TAIR. The radicals could be used as fluorescence quencher for emission due to their activated excited state scavenger role (Gong *et al*., 2014). By monitoring the change of fluorescence spectra of TAID with time at excitation wavelengths to determine the best excitation wavelength from the excitation spectrum, we found that upon repeated excitation of different wavelengths, TAID emission intensity does not change upon continuous 280 excitation (Fig. 8). The fluorescence quantum yield Φ_f of TAID in benzene excited by 280 nm is calculated to 0.052 using anthracene as standard. The corresponding changes in fluorescence of photochromic TAID upon UV irradiation have also been investigated by 280 nm excitation, the intensity at maximum emission wavelength (λ_{em} = 370 nm) decreases rapidly (Fig. 8a).

A after 420 sec UV irradiation, 2 new emission peaks at 367 and 387 nm are observed with decreased intensity (Fig. 9a). Interestingly with decreased intensity, the fluorescence spectra of TAID changes from single peak (λ_{em} = 370 nm) to 2 peaks (λ_{em} = 367 and 387 nm). However, in the dark and due to the thermal recombination reaction of TAIR to TAID, the fluorescence intensity recovers and single peak with emission at 370 nm was observed (Fig. 9b).

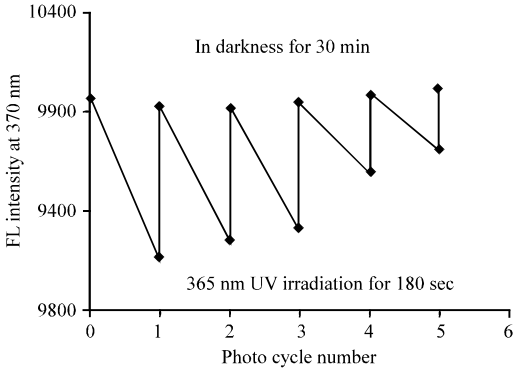

Fig. 10: Fluorescent photoswitching cycles, upon 365 nm irradiation for 180 sec then put in darkness for 30 min as one cycle of TAID (c = 5×10^{-5} M in C_6H_6)

The fluorescence of TAID went up and down reversibly with alternating UV irradiation and darkness, demonstrating the highly efficient photochromism of TAID (Fig. 10). The decrease of fluorescence intensity of TAID after UV irradiation, owing to the formation of nonemissive photoproduct in the form of more flexible radical which open channels of radiationless process. In

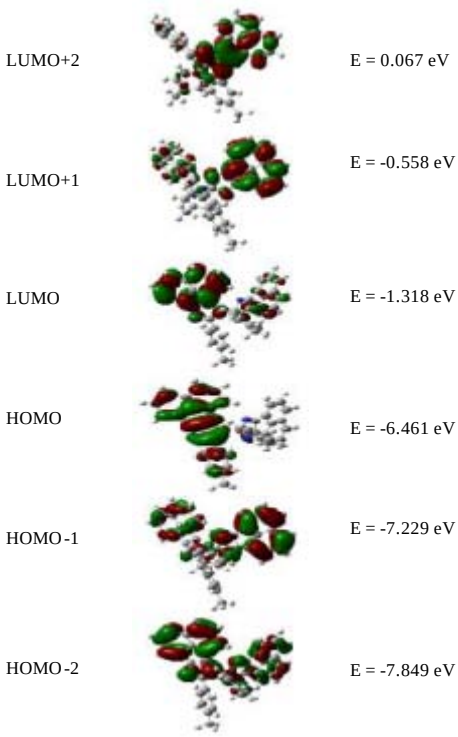

Fig. 11: The HOMO, HOMO-1, HOMO-2, LUMO, LUMO+1 and LUMO+2 of gas-phase TAID which have simulated by using CAM-B3LYP/ 631+G* level of theory

the dark, the intensity recovers due to the thermal recombination reaction of TAIR to TAID. However, the fluorescence intensity at 280 nm excitation was not stable in chloroform.

Frontier Molecular Orbitals (FMOs): The Frontier Molecular Orbitals (FMOs) are formed of the Higher Occupied Molecular Orbitals (HOMOs) and the Lower Unoccupied Molecular Orbitals (LUMOs). The movements of electrons between these FMOs result in $\pi \rightarrow \pi^*$ and $n \rightarrow \pi^*$ electronic transitions (Davis *et al*., 2008). The presence of many double bonds and nitrogen lone pairs on TAID dye facilitate these electronic transitions. CAM-B3LYP/6-31+G* level of theory was used to compute TAID dye gas-phase Frontier Molecular Orbitals (FMOs) (Fig. 11). The LUMO+2 is delocalized over the acenaphthalo-imidazolyl moiety of Im2 as a π^*-antibonding orbital and above the LUMO+1 by 0.625 eV. The later resides above the LUMO by 1.867 eV and extends mainly over the naphthalene moiety of Im2. The LUMO spreads entirely over the acenaphthalo-imidazolyl moiety of Im1 as a π^*-antibonding orbital and above the HOMO by 5.143 eV (acceptor orbital). The HOMO is localized mainly over the imidazolyl moiety of Im1 as π-bonding orbital (donor orbital). The HOMO-1 and HOMO-2 are quite close to each other with an energy difference of 0.620 eV. The former is delocalized over the acenaphthalo-imidazolyl moiety of Im2 while the later extends over the acenaphthalo-imidazolyl moiety of Im1. Both of them are π-bonding donor orbitals. These arrangements facilitate the Intramolecular Charge Transfer (ICT) within the TAID dye. A specific description of the ICT will be shown in a later discussion devoted to Natural Bond Orbital (NBO) analysis. The HOMO and LUMO energies of the gas-phase and solvated TAID dye, together with their energy gaps (E.Gs.) are shown in Table 3. The E.Gs. can be used to evaluate the intermolecular solute-solvent charge transfer. As shown in Table 3, energy gaps of 5.143-5.566 eV which could facilitate the $\pi \rightarrow \pi^*$ and $n \rightarrow \pi^*$ charge transfer which are culminated in the production of UV-Vis. spectra. In addition, the energy gaps of the solvated TAID substrates are directly related to their nature polarities, i.e., their dielectric constants. Compared to gas-phase, both C_6H_6 and $CHCl_3$ stabilize the HOMO but destabilize the LUMO. The stabilization of the HOMO is directly proportional to the solvent polarity while the destabilization of the LUMO is inversely proportional to their dielectric constants. These effects produce small increases of the energy gaps. Table 3 lists the movements of electrons in a chemical species shown by the chemical potential (μ) (Toro-Labbe, 1999) the chemical hardness (η) that computes the stability and reactivity of a chemical species (Pearson, 2005) and the global electrophilicity index (ω) that approximates the stabilizing energy when a chemical species accepts additional electronic charge from the medium (Parr *et al*., 1999). The values of η and μ indicate that TAID dye in $CHCl_3$ is the hardest, most stable and least reactive whilebeing the softer, least stable and most reactive in C_6H_6. Moreover, the magnitude of ω indicate that the solvation of TAID by $CHCl_3$ produces a strong electrophile while being a weak electrophile (or a nucleophile) when solvated by C_6H_6 (Chelli *et al*., 2016).

Natural bond orbital analysis: The delocalization interactions (Reed and Weinhold, 1983) are readily investigated by Natural Bond Orbital (NBO) technique (Reed *et al*., 1988). It is achieved by evaluating second order perturbation energies ($E_{(2)}$) given by the equation:

$$E_{(2)} = \Delta E_{ij} = \frac{q_i \left(F_{ij}\right)^2}{\Delta\varepsilon}$$

Where:

F_{ij} = The NBO Kohn-Sham off-diagonal matrix elements
q_i = The occupancy of the donor orbital (i)
$\Delta\varepsilon$ = Difference between the energies of a donor orbital and an acceptor orbital (j)

Table 3: The HOMO (eV), LUMO (eV) the energy gap (E.G/eV), the electronic chemical potential (μ/eV), the chemical hardness (η/eV), the electrophilicity index (ω/eV) and the 'dipole Moments (D.M./Debye) for the ground state TAID in gas-phase, benzene and choloroform. They have been estimated applying CAM = B3LYP/6-31+G* level fo theory

Parameter	HOMO	LUMO	E.G.	μ	η	ω	D.M.	Dielectric constant
Gas-phase	-6.461	-1.318	5.143	-3..890	2.572	2.942	7.278	1.00
C_6H_6	-6.723	-1.282	5.441	-4.003	2.721	2.945	8.623	2.27
$CHCI_3$	-6.866	-1.300	5.566	-4.083	2.783	2.995	9.363	4.81

Table 4: Some selected second order perturbation ($E_{(2)}$) hyperconjugative energies (kcal/mol) of the TAID which were computed by using HF/321G/CAM-B3LY/6-31+G* level of theory

Im1 intercations	Energy	Subtotal	Im2 interactions	Energy
$\pi_{C1-C2}\rightarrow\pi^*_{C5-C6}$	31.19		$\pi_{C21-C22}\rightarrow\pi^*_{C23-C24}$	32.06
$\pi_{C5-C6}\rightarrow\pi^*_{C11-C12}$	18.16		$\pi_{C21-C2}\rightarrow\pi^*_{C33-N4}$	23.41
$\pi_{C7-C10}\rightarrow\pi^*_{C8-C9}$	29.75		$\pi_{C33-N4}\rightarrow\pi^*_{C32-N3}$	17.44
$\pi_{C11-C12}\rightarrow\pi^*_{C13-N2}$	29.33		$\pi_{C34-C35}\rightarrow\pi^*_{C36-C37}$	37.20
$\pi_{C13-N2}\rightarrow\pi^*_{C11-C12}$	39.72	197.87	$\pi_{C34-C35}\rightarrow\pi^*_{C38-C39}$	47.18
$\pi_{C13-N2}\rightarrow\pi^*_{C14-C16}$	05.79		$\pi_{C36-C37}\rightarrow\pi^*_{C34-C35}$	44.40
$\pi_{C14-C16}\rightarrow\pi^*_{C15-C18}$	43.93		$\pi_{C36-C37}\rightarrow\pi^*_{C38-C39}$	38.93
$n_{1N1}\rightarrow\pi^*_{C11-C12}$	56.76	130.45	Total	240.60
$n_{1N1}\rightarrow\pi^*_{C13-N2}$	73.69			

The second order perturbation ($E_{(2)}$) hyperconjugative energies of gas-phase TAID dye that follow the charge transfer from the donor acetophthalo-imidazolyl ring to the toluene moiety acceptor are listed in Table 4. They were estimated by using HF/321G/CAM-B3LYP/6-31+G* level of theory. They originate from the $\pi\rightarrow\pi^*$ and $n\rightarrow\pi^*$ charge transfer interactions. It appears from Table 4 and Fig. 2, that these delocalization interactions occur only within each tolyl-acenaphthalo-imidazolyl species. That is the hyperconjugative interactions do not exist between Im1 and Im2. This finding is supported by the existence of a single C-N bond (1.478Å) between 1 and Im2.

For the semi-planar Im1 there exists some charge transfer within the acenaphthalo-imidazolyl ring and from the acenaphthalo-imidazolyl moiety as a donor to the tolyl species as an acceptor. These interactions are exemplified by the $n_{1N1}\rightarrow\pi^*_{C11-C12,}$ $n_{1N1}\rightarrow{}^*C_{13-N2}$ and $\pi_{C13-N2}\rightarrow\pi^*_{C14-C16}$ interactions that availed 56.76, 73.69 and 5.79 kcal/mol, respectively for the stabilization of TAID dye. The later interaction is supported by a shorter than expected C13-C14 of 1.477Å. Those kinds of delocalization interactions do not occur for Im2 due to the lack of planarity. Therefore, the hyperconjugative interactions occur solely within each of its components. On the one hand, the delocalization interactions that occur within the acenaphthalo-imidazolyl include $\pi^*_{C21-C22}\rightarrow\pi^*_{C23-C24,}$ $\pi^*_{C21-C22}\rightarrow\pi^*_{C33-N4}$ and $\pi^*_{C33-N4}\rightarrow\pi^*_{C32-N3}$ which contributed energies of 32.06, 23.41 and 17.44 kcal/mol to the stability of TAID dye. On the other hand, the ones that dwell the tolyl moiety comprise $\pi^*_{C34-C35}\rightarrow\pi^*_{C38-C39,}$ $\pi^*_{C34-C35}\rightarrow\pi^*_{C38-C39,}$ $\pi^*_{C36-C37}\rightarrow\pi^*_{C34-C35}$ and $\pi^*_{C36-C37}\rightarrow\pi^*_{C38-C39}$ with stabilization energies of 37.20, 48.18, 44.40 and 38.93 kcal/mol, respectively. These results facilitate our observed UV-V is spectra.

CONCLUSION

The synthesis of 1, 2'-isomer structure of TAID molecular switches is described as well as their photochromic, fluorescence switching and fatigue resistance. A kinetic study of synthesized TAID shows that the photo-coloration and thermal bleaching processes obey first and second-order rate equations, respectively and the switching speed of the photochromic compounds is generally a .ected by the solvent.

ACKNOWLEDGEMENT

The researchers are thankful to the King Abdulaziz City for Science and Technology (KACST) for providing the financial support for this researche (No. 1-17-01-009-0046).

REFERENCES

Asiri, A.M. and K.O. Badahdah, 2006. Synthesis photochromic thermochromic piezochromic and solvatochromic properties of new bis-Imidazole derived from substituted chlorobenzaldehyds. Pigm. Res. Technol., 35: 200-204.

Asiri, A.M., G.A. Baghaffar, K.O. Badahdah, A.G. Al-Sehemi and S.A. Khan *et al.*, 2009. Multifunctional switches based on bis-Imidazole derivative. J. Chem. Sci., 121: 983-987.

Asiri, A.M., K.O. Badahdeh, K.A. AlAmry and A.A. Bukhari, 2005. Synthesis, photochromic, thermochromic, piezochromic and solvatochromic properties of new bis-Imidazol. Chem., 2: 5-10.

Bahajaj, A.A. and A.M. Asiri, 2007. Photocoloration and photobleaching of 3-(2-Adamantylidene) -2-[5-(p-Diethylamino) phenyl-2-Methyl-3-Furylethylidene]-Succinic anhydride doped in PMMA polymer film. J. Photochem. Photobiol. A: Chem., 191: 182-186.

Bandara, H.D. and S.C. Burdette, 2012. Photoisomerization in different classes of azobenzene. Chem. Soci. Rev., 41: 1809-1825.

Bulanov, A.O., B.B. Safoklov, B.S. Luk'yanov, V.V. Tkachev and V.I. Minkin *et al*., 2003. Photochromic and thermochromic spiropyrans. 22. Spiropyrans of the 4-Oxo-3, 4-dihydro-3h-1, 3-benzoxazine series containing p-accepting substituents at position 8. Chem. Heterocycl. Compd., 39: 315-317.

Cances, E., B. Mennucci and J. Tomasi, 1997. A new integral equation formalism for the polarizable continuum model: Theoretical background and applications to isotropic and anisotropic dielectrics. J. Chem. Phys., 107: 3032-3041.

Chelli, S., K. Troshin, P. Mayer, S. Lakhdar and A.R. Ofial *et al*., 2016. Nucleophilicity parameters of stabilized Iodonium ylides for characterizing their synthetic potential. J. Am. Chem. Soc., 138: 10304-10313.

Coelho, P.J., M.A. Salvador, B.M. Heron and L.M. Carvalho, 2005. Spectrokinetic studies on new bi-photochromic molecules containing 2 naphthopyran entities. Tetrahedron, 61: 11730-11743.

Cohen, R.L., 1971. Substituent effects on the reactivity of triarylimidazolyl free radicals toward tris (2-Methyl-4-Diethylaminophenyl) methane. J. Org. Chem., 36: 2280-2284.

Coraor, G.R., L.A. Cescon, R. Dessauer, E.F. Silversmith and E.J. Urban, 1971. Properties of triarylimidazolyl radicals and their dimers. J. Org. Chem., 36: 2262-2267.

Corns, S.N., S.M. Partington and A.D. Towns, 2009. Industrial organic photochromic dyes. Color. Technol., 125: 249-261.

Davis, N.K.S., M. Pawlicki and H.L. Anderson, 2008. Expanding the porphyrin p-System by fusion with anthracene. Org. Lett., 10: 3945-3947.

Dessauer, R., 2006. Photochemistry History and Commercial Applications of Hexaarylbiimidazoles: All about HABIs. Elsevier, Amsterdam, Netherlands, ISBN-13:978-0-444-52770-7, Pages: 235.

Edkins, R.M., M.R. Probert, C.M. Robertson, J.A. Howard and A. Beeby, 2014. Photocrystallisation of the 2C-2'C dimer of a triphenylimidazolyl radical. RSC. Adv., 4: 5351-5356.

Frisch, M., G. Trucks, H. Schlegel, G. Scuseria and M. Robb *et al*., 2009. Gaussian 09, Revision A. 02, 2009. Gaussian Inc., Wallingford, Connecticut,.

Gong, W.L., Z.J. Xiong, C. Li and M.Q. Zhu, 2014. Design synthesis and photoswitching of broad-Spectrum fluorescent hexaarylbiimidazoles. RSC. Adv., 4: 64371-64378.

Gross, E.K.U. and W. Kohn, 1990. Time-dependent density-functional theory. Adv. Quantum Chem., 21: 255-291.

Hatano, S., K. Sakai and J. Abe, 2010. Unprecedented radical-Radical reaction of a [2.2] Paracyclophane derivative containing an imidazolyl radical moiety. Org. Lett., 12: 4152-4155.

Irie, M., 2000. Diarylethenes for memories and switches. Chem. Rev., 100: 1685-1716.

Islamova, N.I., X. Chen, S.P. Garcia, G. Guez and Y. Silva *et al*., 2008. Improving the stability of photochromic fluorinated indolylfulgides. J. Photochem. Photobiol. A. Chem., 195: 228-234.

Iwasaki, T., T. Kato, Y. Kobayashi and J. Abe, 2014. A chiral BINOL-Bridged imidazole dimer possessing sub-Millisecond fast photochromism. Chem. Commun., 50: 7481-7484.

Kikuchi, A., T. Iyoda and J. Abe, 2002. Electronic structure of light-Induced lophyl radical derived from a novel hexaarylbiimidazole with p-Conjugated chromophore. Chem. Commun., 14: 1484-1485.

Koko, M. and H. Taro, 1970. The mechanism of photochromism, thermochromism and piezochromism of dimers of triarylimidazolyl. Bull. Chem. Soc. Jpn., 43: 429-438.

Koshima, H., K. Takechi, H. Uchimoto, M. Shiro and D. Hashizume, 2011. Photomechanical bending of salicylideneaniline crystals. Chem. Commun., 47: 11423-11425.

Masaki, K., S. Tomokatsu, A. Jiro and O. Yuji, 2000. In situ observation of molecular swapping in a crystal by X-Ray analysis. Chem. Lett., 29: 1372-1373.

Milliam, J., A. Nielsen, A. Holder and J. Hiscocks, 2007. Gauss View Reference, Version 4.0. Gaussian Inc, Pittsburgh, Pennsylvania,.

Mutoh, K., E. Nakano and J. Abe, 2012. Spectroelectrochemistry of a photochromic [2.2] paracyclophane-bridged imidazole dimer: Clarification of the electrochemical behavior of HABI. J. Phys. Chem. A, 116: 6792-6797.

Nakamura, S. and M. Irie, 1988. Thermally irreversible photochromic systems, a theoretical study. J. Org. Chem., 53: 6136-6138.

Nithyanandan, S. and P. Kannan, 2013. Photo switchable pendant furyl and thienyl fulgimides containing polypyrroles. Polym. Degrad. Stab., 98: 2224-2231.

Ohshima, S., M. Morimoto and M. Irie, 2015. Light-driven bending of diarylethene mixed crystals. Chem. Sci., 6: 5746-5752.

Parr, R.G., L.V. Szentplay and S. Liu, 1999. Electrophilicity index. J. Am. Chem. Soc., 121: 1922-1924.

Pearson, R.G., 2005. Chemical hardness and density functional theory. J. Chem. Sci., 117: 369-377.

Radziszewski, B.R., 1877. [Studies on hydrobenzamide, amarin and lophin (In German)]. Ber. Der Dtsch. Chem. Ges., 10: 70-75.

Reed, A.E. and F. Weinhold, 1983. Natural bond orbital analysis of near-Hartree-Fock water dimer. J. Chem. Phys., 78: 4066-4073.

Reed, A.E., L.A. Curtiss and F. Weinhold, 1988. Intermolecular interactions from a natural bond orbital donor-Acceptor viewpoint. Chem. Rev., 88: 899-926.

Reed, A.E., L.A. Curtiss and F. Weinhold, 1988. Intermolecular interactions from a natural bond orbital, donor-Acceptor viewpoint. Chem. Rev., 88: 899-926.

Robert, F., A.D. Naik, F. Hidara, B. Tinant and R. Robiette *et al*., 2010. Engineering solid-state molecular switches: N-salicylidene N-heterocycle derivatives. Eur. J. Org. Chem., 2010: 621-637.

Shirinian, V.Z., A.G. Lvov, M.M. Krayushkin, E.D. Lubuzh and B.V. Nabatov, 2014. Synthesis and comparative photoswitching studies of unsymmetrical 2, 3-Diarylcyclopent-2-En-1-ones. J. Org. Chem., 79: 3440-3451.

Slavov, C., N. Bellakbil, J. Wahl, K. Mayer and K. Ruck-Braun *et al*., 2015. Ultrafast coherent oscillations reveal a reactive mode in the ring-Opening reaction of fulgides. Phys. Chem. Chem. Phys., 17: 14045-14053.

Toro-Labbe, A., 1999. Characterization of chemical reactions from the profiles of energy chemical potential and hardness. J. Phys. Chem. A., 103: 4398-4403.

White, D.M. and J. Sonnenberg, 1966. Oxidation of triarylimidazoles: Structures of the photochromic and piezochromic dimers of triarylimidazyl radicals. J. Am. Chem. Soc., 88: 3825-3829.

Yamaguchi, T., M.F. Hilbers, P.P. Reinders, Y. Kobayashi and A.M. Brouwer *et al*., 2015. Nanosecond photochromic molecular switching of a biphenyl-Bridged imidazole dimer revealed by wide range transient absorption spectroscopy. Chem. Commun., 51: 1375-1378.

Yanai, T., D.P. Tew and N.C. Handy, 2004. A new hybrid exchange-correlation functional using the Coulomb-Attenuating Method (CAM-B3LYP). Chem. Phys. Lett., 393: 51-57.

Zhu, M.Q., G.F. Zhang, C. Li, M.P. Aldred and E. Chang *et al*., 2010. Reversible two-Photon photoswitching and two-Photon imaging of immunofunctionalized nanoparticles targeted to cancer cells. J. Am. Chem. Soc., 133: 365-372.

Zhu, M.Q., G.F. Zhang, C. Li, Y.J. Li and M.P. Aldred *et al*., 2011. Photoswitchable nanofluorophores for innovative bioimaging. J. Innovative Opt. Health Sci., 4: 395-408.